SPEI-BASED DROUGHT PROJECTIONS FOR UGANDA UNDER CLIMATE CHANGE SCENARIOS USING THE CANESM5 CMIP6 MODEL

***Obed BYAMUKAMA*[1], *Ronald SSEMBAJWE*[2,3], *Mihai VODA*[4*] & *Brian Odhiambo AYUGI*[5]**

DOI: 10.21163/GT_2026.211.11

ABSTRACT

Drought is one of the most recurrent and damaging climate extremes in Uganda, affecting agriculture, water resources, and livelihoods. However, its future trends under changing climate conditions remain poorly understood. This study analyzed historical and projected drought characteristics across Uganda. We used the Standardized Precipitation–Evapotranspiration Index (SPEI) derived from the bias-corrected CanESM5 model within the NASA Earth Exchange Global Daily Downscaled Projections (NEX-GDDP-CMIP6) framework. Three Shared Socioeconomic Pathways (SSP1-2.6, SSP2-4.5, and SSP5-8.5) representing low, medium, and high emissions scenarios were considered. Terra-Climate data for 1985–2014 were used for bias correction and validation. Drought duration, frequency, severity, and intensity were calculated from 3-month SPEI, and spatial clustering was assessed using the Getis-Ord Gi* statistic. Historical analysis shows drying trends in northern and central Uganda. Future projections reveal spatially heterogeneous drought responses. During the mid-century (2041–2070), drought occurrence increases under SSP1-2.6 in central and northern regions but decreases under SSP2-4.5 in the central-west and under SSP5-8.5 in Karamoja. Toward the late century (2071–2100), SSP1-2.6 indicates a general decline in drought occurrence, SSP2-4.5 shows increasing droughts in the east and reductions in the northwest, and SSP5-8.5 projects widespread intensification across southern, western, and northern Uganda. Hotspot analysis identifies persistent drought clusters along the cattle corridor, extending from the Ankole–Kigezi regions and Karamoja. These findings provide a detailed understanding of Uganda's evolving drought risks and support targeted adaptation planning, water resource management, and climate-resilient livelihood strategies.

Keywords: *Climate models; Drought projection; SPEI; NEX-GDDP-CMIP6; Uganda.*

1. INTRODUCTION

Droughts are among the most complex and devastating environmental hazards worldwide, evolving slowly yet with long-lasting ecological and socioeconomic consequences. Unlike sudden extreme events such as floods or hurricanes, droughts evolve slowly, persisting for months or years and affecting vast areas (Krishna Prabhakar, 2022; Orimoloye et al., 2022). Their gradual onset makes detection, monitoring, and management particularly challenging. Intensifying climate change is projected to exacerbate both the frequency and severity of droughts, heightening risks for vulnerable regions (IPCC, 2022).

[1]*Department of Natural Resources and Environmental Management, IPB University, Bogor 16680, Indonesia, byamukamaobed@apps.ipb.id*
[2]*College of Agricultural and Environmental Sciences, Makerere University, P.O. Box 7062 University Rd, Kampala, Uganda, nazirte.sronald@yahoo.ca*
[3]*National Coffee Research Institute, National Agricultural Research Organization, P.O. Box 185, Mukono, Uganda*
[4]*Faculty of Geography, Dimitrie Cantemir University, Bodoni Sándor Street 3–5, Târgu Mureș, Romania.*
** Corresponding author: mihaivoda@cantemir.ro*
[5]*East African Hub, Wyss Academy for Nature at the University of Bern, Nanyuki 10400, Kenya, ayugi.o@gmail.com*

Sub-Saharan Africa faces a disproportionate drought burden due to structural vulnerabilities such as poverty, dependence on rainfed agriculture, and limited adaptive capacity (Lombe et al., 2024; Voda et al., 2019). Recurrent droughts have reduced agricultural productivity, disrupted livelihoods, and deepened food insecurity (Onyeaka et al., 2024). These events also drive water scarcity and rural-urban migration. This intensifies competition for limited resources and puts pressure on urban infrastructure (Calverley and Walther, 2022; Ceola et al., 2023; Li et al., 2023). Recent studies indicate an upward trend in drought frequency and intensity across Africa, driven by reduced precipitation and rising evapotranspiration (Elkouk et al., 2021; Han et al., 2022; Mathivha et al., 2024; Orke and Li, 2022; Satoh et al., 2022; R Ssembajwe, Nguefack, et al., 2025; Uwimbabazi et al., 2022).

Uganda exemplifies this regional vulnerability. Nearly 80 percent of households in Uganda rely on agriculture as their main economic activity (UBOS, 2024), and most of this agriculture is rainfed. As a result, the country's economy and food systems are highly sensitive to rainfall variability. Despite the increasing frequency and impacts of drought, most research efforts in Uganda have remained localized, focusing on specific districts or regions and relying largely on a single meteorological variable such as precipitation (Byakatonda et al., 2021; Kyatengerwa et al., 2020; Mulinde et al., 2016; Najjuma et al., 2021; Nakalembe, 2018; Nalwanga et al., 2024; Onyutha and Kerudong, 2022). While such studies provide valuable local insights, they lack the spatial continuity, resolution, and bias correction consistency required for robust national-scale projections (Voda AI et al., 2018). Furthermore, it is not clear how the projected warming will affect regional and local water balances especially in countries like Uganda where the vulnerability is high.

The availability of advanced downscaled climate model datasets now provides new opportunities to address these limitations. The NASA Earth Exchange Global Daily Downscaled Projections based on CMIP6 (NEX-GDDP-CMIP6) is one such datasets. This dataset offers bias-corrected and statistically downscaled data for up to 16 climate variables at approximately 25 km spatial resolution for the period 1950–2100 (Thrasher et al., 2022). It has been successfully applied in several regions to assess hydrological and climatic extremes. For example, it has been used to project rainfall variability in the Brazilian Amazon and Cerrado (de Mendonça et al., 2024), temperature and precipitation changes in China (Wu et al., 2023), and extreme weather indices across the Arabian Peninsula and the UAE (Baogang et al., 2024; Rao et al., 2024; Vinodhkumar et al., 2024). In Africa, it has demonstrated skill in reproducing observed precipitation patterns, though regional performance varies with the reference dataset used (Samuel et al., 2025). In Uganda, (Ronald Ssembajwe et al., 2025) used it to track future atmospheric circulations such as wind and humidity. However, its potential in simulating droughts especially based on the water balance remains largely unexplored in Uganda.

This study employs the bias-adjusted and statistically downscaled NEX-GDDP-CMIP6 CanESM5 model to project future drought dynamics in Uganda based on scale 3 SPEI. Specifically, it aims to (1) simulate and validate historical droughts using TerraClimate-based SPEI droughts as a reference, (2) analyse historical and future drought characteristics and long-term trends based on SSP1-2.6, SSP2-4.5 and SSP5-8.5, and (3) identify historical and future spatial drought hotspots. By integrating advanced CMIP6 projections with observational datasets, this study provides new insights to inform climate-resilient development, drought preparedness, and formulation of effective national adaptation strategies.

2. STUDY AREA

This study was conducted in Uganda, an inland country located in East Africa along the equator (Byamukama et al., 2025). It lies between longitudes 29°E and 35.2°E and latitudes 4.5°N and 1.5°S (**Fig. 1**). Uganda covers 241,551 km² (UBOS, 2025) and is bordered by Kenya, South Sudan, the Democratic Republic of Congo, Tanzania, and Rwanda.

The country's terrain is diverse, consisting of elevated plateaus, highlands, and extensive wetlands. Prominent features include the Rwenzori Mountains in the west, Mount Elgon in the east, and the Albertine Rift Valley. Major lakes such as Victoria, Kyoga, and Albert, together with the

River Nile, play a key role in influencing local convection and humidity, resulting in spatial variability in rainfall patterns.

Uganda's climate is shaped by the seasonal migration of the Intertropical Convergence Zone (ITCZ), monsoon systems, and large-scale circulation patterns (Jury, 2018). The country experiences a bimodal rainfall regime, with the long rains from March to May (MAM) and short rains from September to November (SON) (Ngoma et al., 2021). Annual rainfall ranges from about 500 mm in the semi-arid northeast to more than 2,000 mm in the southern and western highlands (Nuwagira and Yasin, 2022). The mean near-surface annual temperature is approximately 21°C, with monthly values ranging from 15°C in July to 30°C in February (Nsubuga and Rautenbach, 2018).

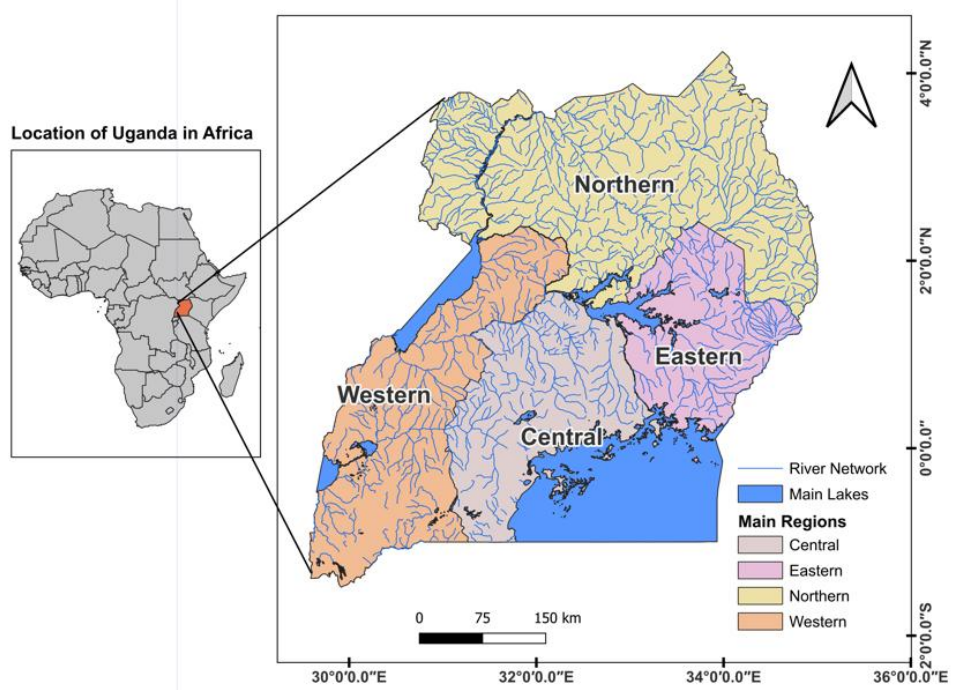

Fig. 1. Map showing location of Uganda in Africa, the four major regions, major lakes, and river networks that influence regional climatic and hydrological patterns.

3. DATA AND METHODS

3.1. Data acquisition

3.1.1. CanESM5 projected data

We used NEX-GDDP-CMIP6, the latest version of NASA's global downscaled climate projection product. NEX-GDDP-CMIP6 provides bias-corrected and statistically downscaled daily climate projections from CMIP6 models at a 0.25° × 0.25° (~25 km) spatial resolution (Thrasher et al., 2022). The NEX-GDDP scheme uses the bias correction and statistical downscaling (BCSD) method to downscale global climate models (GCMs) from parent coarse resolutions ranging from 1◦ × 1◦ to 2.5◦ × 2.5◦ to a finer 0.25◦ × 0.25◦ (Ronald Ssembajwe et al., 2025). The dataset covers a reference period (1950–2014) and future projections (2015–2100) under Shared Socioeconomic Pathways (SSP1-2.6, SSP2-4.5, SSP3-7.0, and SSP5-8.5). For consistency with TerraClimate, the 1985–2014 period was used as the reference period. The dataset is publicly available through NASA's Earth Exchange platform at https://ds.nccs.nasa.gov/thredds/catalog/AMES/NEX/GDDP-CMIP6/catalog.html.

For this study, we selected CanESM5 model based on its demonstrated skill in reproducing East African climate regimes and their associated drivers such as El Nino Southern Oscillations, Dipole modes and orientation and strength of high-pressure cells (Ayugi et al., 2022; Dufatanye Umwali et al., 2024). Thus, we obtained CanESM5 daily downscaled and bias-corrected climate variables from the NEX-GDDP-CMIP6 archive for SPEI computation. This included precipitation (P) and mean air temperature, relative humidity (RH), 2-m wind speed, and downwelling shortwave radiation. All data were accessed in NetCDF format for both the historical (1985–2014) and future (2041–2070 and 2071–2100) periods. Although multi-model ensembles provide a wider uncertainty range (Akinsanola et al., 2021), we used a single, well-performing earth systems model. This allowed a detailed bias-adjusted analysis while ensuring computational efficiency in dataset handling.

3.1.2. CanESM5 projected data

Monthly precipitation and potential evapotranspiration (PET) from TerraClimate were used as reference data for model validation and bias correction. TerraClimate provides globally consistent 4 km gridded climate data. It integrates the University of East Anglia CRU TS dataset, JRA-55 reanalysis, and WorldClim datasets, effectively capturing both long-term climatological means and monthly anomalies (Abatzoglou et al., 2018). Its integration of ground, satellite, and reanalysis data ensures high consistency and spatial detail, making it well-suited for regional drought analysis, particularly in data-sparse regions such as Uganda. TerraClimate has been widely validated and shown to perform well against station-based and reanalysis datasets, making it suitable for near-surface climate variability and water balance studies (Kolling Neto et al., 2024). For East Africa, studies like Kobusinge et al., (2024) and Ronald Ssembajwe et al., (2025) have relied on it for hydrological and agroclimatic assessments. A recent validation study against station observations by R Ssembajwe, Ngatia, et al., (2025) has shown Terra-Climate's reliability in reproducing the climatology of hydrothermal variables such as temperature, humidity and vapor pressure deficit over East Africa thus, justifying its adoption.

The dataset was accessed at http://www.climatologylab.org/terraclimate.html. Additionally, the ASTER Global Digital Elevation Model (DEM) at 30 m spatial resolution was used to derive surface atmospheric pressure for the FAO-56 Penman–Monteith PET computation.

3.2. Preprocessing

3.2.1. Data curation and quality control

All climate datasets were processed within the MATLAB R2025b environment. The NEX-GDDP-CMIP6 data were obtained as single year NetCDF files and concatenated into continuous 30-year time series for each climate variable per period: 1985-2014, 2041-2070 and 2071-2100. The datasets were then spatially subset and masked to Uganda's administrative boundaries using MATLAB's spatial masking tools. Because the NEX-GDDP-CMIP6 grid (~25 km) differed from the Terra-Climate grid (~4 km), a second-order conservative regridding technique was applied to align the CanESM5 data with the reference Terra-Climate resolution. We then explored the datasets for completeness and validity using isnan function and logical operators, respectively. The completeness test indicated no missing values.

3.2.2. Computation of PET and SPEI

3.2.2.1. Potential Evapotranspiration

The modified FAO56 (Penman-Monteith) method (equation 1) was applied to compute historical simulated and future PET using daily air mean temperature, RH, downwelling shortwave radiation, windspeed, and surface pressure derived from the DEM. We chose FAO56 because of its robustness over humid equatorial regions like Uganda (Ssembajwe et al., 2024), and its global recommendation as the empirical standard for PET computation (Allen et al., 1998). The FAO56 Penman-Monteith equation is expressed as:

$$PET = \frac{0.408\Delta(R_n - G) + \gamma \frac{900}{T + 273} U_2(e_s - e_a)}{\Delta + \gamma(1 + 0.34u_2)} \quad (1)$$

where PET is the potential evapotranspiration (mm day^{-1}), Rn is the net radiation at the crop surface (MJ m^{-2} day^{-1}), G is soil heat flux density (MJ m^{-2} day^{-1}), T is mean daily air temperature at 2 m height (°C), u_2 is wind speed at 2 m height (m s^{-1}), e_s is saturation vapor pressure (kPa), e_a is actual vapor pressure (kPa), ($e_s - e_a$) is vapor pressure deficit (kPa), Δ is slope of the saturation vapor pressure–temperature curve (kPa °C^{-1}) and γ is psychrometric constant (kPa °C^{-1}). All intermediate parameters were computed following the FAO-56 guidelines (Allen et al., 1998).

Daily PET and precipitation from CanESM5 were aggregated to monthly means to maintain temporal consistency with TerraClimate. The process involves binning daily precipitation and PET datasets into annual and monthly cycles based on the time/datetime vector corresponding to each dataset using the unique function in MATLAB (R Ssembajwe, Twah, et al., 2025). The outputs are then reshaped to the original dimensions and aggregated according to each month's length using a for loop. The resulting monthly PET and precipitation series were subsequently used in the computation of SPEI.

3.2.2.2. Standardized Precipitation-Evapotranspiration Index (SPEI)

SPEI, developed by Vicente-Serrano et al., (2010), is a widely applied multiscalar drought index that integrates both precipitation and PET to provide a more comprehensive measure of drought conditions. Unlike the Standardized Precipitation Index (SPI), which relies solely on precipitation, SPEI incorporates temperature-driven evapotranspiration, making it particularly relevant for assessing droughts under a changing climate (Vicente-Serrano et al., 2010; Wang et al., 2021). Its sensitivity to both moisture deficits and warming trends allows it to detect drought onset, persistence, and intensity across multiple timescales, from short-term agricultural droughts to long-term hydrological droughts (Wang et al., 2021).

In this study, we applied SPEI at a 3-month timescale (SPEI-03) to account for vegetation's delayed response to shocks and seasonal variability. This choice reflects Uganda's bimodal rainfall regime, where the March–May and September–November rainy seasons are critical for agriculture and water availability. Shorter timescales (1–3 months) have been shown to effectively characterize meteorological and agricultural droughts, which directly impact soil moisture and crop production (Vicente-Serrano et al., 2010). Previous East African drought studies have also adopted 3-month drought indices to assess seasonal drought dynamics in regions with strong rainfall seasonality (Ayugi et al., 2022).

The SPEI was computed by first estimating the monthly climate water balance, D, as the difference between precipitation (P) and PET (equation 2).

$$D = P - PET \quad (2)$$

where D is the monthly water balance (deficit or surplus in mm), P is the total monthly precipitation (mm), and PET is the potential evapotranspiration for the same month (mm). Positive values of D indicate moisture surplus (conditions are wetter than normal), while negative values reflect deficits, signifying drought conditions.

The accumulated water balance series (D) were fitted to a log-logistic probability distribution, following Vicente-Serrano et al., (2010). The probability density function is expressed as in equation (3).

$$f(x) = \frac{\beta}{\alpha}\left(\frac{x - \gamma}{\alpha}\right)\left[1 + \left(\frac{x - \gamma}{\alpha}\right)\right]^{-2} \quad (3)$$

where f(x) is the cumulative probability function of x (the water balance deficit D), α, β, and γ are the scale, shape, and location parameters of the distribution, respectively for D values in the range ($\gamma < x < \infty$).

Parameters of the log-logistic distribution can be estimated following the L-moment procedure (Ahmad et al., 1988). Hence, the probability distribution function of the D series, according to the log-logistic distribution, is given by equation (4).

$$F(x) = \left[1 + \left(\frac{\alpha}{x - \gamma}\right)^{\beta}\right]^{-1} \quad (4)$$

After fitting the distribution, the water balance values are transformed into standardized SPEI values. These standardized values enable comparisons across different time periods and regions. As described by Vicente-Serrano et al., (2010), the SPEI is obtained by standardizing values of $F(x)$ as in equation (5)

$$SPEI = w - \frac{c_0 + Cw + C_2 w^2}{1 + d_1 w + d_2 w^2 + d_3 w^3} \quad (5)$$

when $P \leq 0.5$, $w = \sqrt{-2\,ln(P)}$ and when $P > 0.5$, $w = \sqrt{-2\,ln(1-P)}$

where C0 = 2.5155, C1 = 0.802853, C2 = 0.010328, d1 = 1.432788, d2 = 0.189269, and d3 = 0.001308. All these parameters are defined in the study by Vicente-Serrano et al., (2010).

The negative and positive SPEI values indicate dry and wet conditions, respectively. **Table 1** summarizes the category of dry and wet conditions based on SPEI values following the description by Mckee et al., (1993).

Table 1

Categories of dry and wet conditions indicated by SPEI values.

SPEI value	Category
2 and above	Extremely wet
1.5 to 1.99	Very wet
1.0 to 1.49	Moderately wet
-0.99 to 0.99	Near normal
−1.0 to −1.49	Moderately dry
-1.5 to -1.99	Severely dry
-2 and less	Extremely dry

3.3. Data analysis

3.3.1. Empirical Quantile Mapping (EQM) for SPEI bias correction

Although the NEX-GDDP-CMIP6 data used for SPEI computation were already downscaled and bias-corrected, we applied an additional correction to further align CanESM5-simulated SPEI values with the TerraClimate-based SPEI. This was achieved using the EQM technique.

EQM corrects systematic deviations by mapping the cumulative distribution function (CDF) of the model outputs to that of the reference dataset (Li et al., 2023; Niranjan Kumar et al., 2022; Ernawati et al., 2018). Unlike parametric approaches, EQM does not assume a specific theoretical distribution for the data (Niranjan Kumar et al., 2022). This makes it suitable for climate variables such as precipitation and SPEI that often exhibit skewed or multimodal behavior. Mathematically, the bias-adjusted value x_a can be expressed by equation (6).

$$x_a = F_o^{-1}\left(F_m(x_m)\right) \quad (6)$$

where F_m and F_o^{-1} and represent the empirical cumulative distribution and its inverse for the model and observed datasets, respectively.

The corrected SPEI outputs were validated against TerraClimate-based SPEI for the historical period using histogram and kernel density estimation (KDE) plots. This helped to assess distributional consistency. It was also validated through grid-level time series comparisons to evaluate temporal coherence.

3.3.2. Drought characteristics

Drought events were identified using the run theory approach as proposed by Li et al. (Yevjevich, 1967). A run is the portion of all values in a time series that is below or above a cutoff threshold. Here, sequences of consecutive periods during which the drought index remained below -1 (SPEI ≤ –1) were isolated. Each continuous sequence below this threshold was defined as a single drought event, beginning at the onset (first month below –1) and ending when SPEI exceeded –1. This approach allowed for the systematic identification and quantification of individual drought events from a continuous SPEI time series. After identifying drought events, key drought characteristics including duration, severity, intensity, and frequency were computed using equations (7–10).

i. Drought Duration (DD) refers to the number of consecutive months from onset (SPEI≤-1) until cessation (SPEI > -1). Average drought duration across the study period was calculated using equation (7).

$$\overline{DD} = \frac{\sum_{i=1}^{N} DDi}{N} \tag{7}$$

where i is the event and *N* is the total number of drought events

ii. Drought Severity (DS) refers to the cumulative magnitude of drought over its duration, defined as the absolute sum of SPEI values below the threshold as in equation (8).

$$\mathrm{DS} = \sum_{t=t_{stat}}^{t_{end}} |SPEI_t| \tag{8}$$

where $\boldsymbol{S}PEI_t$ is the SPEI value at time t and *N* is the duration of the drought in months

iii. Drought Intensity (DI) refers to the average severity per month during a drought event and is given by equation (9).

$$DI = \frac{DS}{DD} \tag{9}$$

iv. Drought Frequency (DF) refers to the number of drought events relative to the length of the study period, given by equation (10).

$$DF = \frac{Number\ of\ drought\ events}{Total\ number\ of\ months} \tag{10}$$

3.3.3. Hotspot analysis

Spatial hotspots of drought intensity and frequency were identified using the Getis-Ord Gi* statistic (Getis and Ord, 1992) implemented, in MATLAB R2025b. The method detects statistically significant clusters by comparing the local sum of each grid cell and its neighbors to the global mean of the study area (Nejadrekabi et al., 2021; Rousta et al., 2017). The Gi* statistic measures whether high or low values occur together in space more often than would be expected by random chance, thereby highlighting hotspots (clusters of high drought values) and coldspots (clusters of low drought values). The Getis-Ord Gi* statistic is given by Equation (11) with its terms defined by equations (12) and (13).

$$G_i^* = \frac{\sum_{j=1}^{n} w_{ij}x_j - \bar{x}\sum_{j=1}^{n} w_{ij}}{S\sqrt{\frac{n\sum_{j=1}^{n} w_{ij} - \left(\sum_{j=1}^{n} w_{ij}\right)^2}{n-1}}} \quad (11)$$

$$\bar{X} = \frac{1}{n}\sum_{j=1}^{n} x_j \quad (12)$$

$$S = \sqrt{\frac{1}{n}\sum_{j=1}^{n} x_j^2 - (\bar{x})^2} \quad (13)$$

where G_i^* is the Getis-Ord local statistic for location i, x_j is the drought variable value at location j. w_{ij} is the spatial weight between locations i and j, n is the total number of locations (grid cells), $\bar{X}$ is the mean of all x_j and S is the standard deviation of x_j. The weights w_{ij} define spatial proximity based on a fixed-distance band, such that nearby grid cells exert stronger influence on Gi* values.

Each grid cell receives a Z-score indicating the degree of spatial clustering. High positive Z-scores denote hotspots (areas with significantly high drought values), whereas negative Z-scores indicate coldspots (areas with low drought values). Z-scores close to zero reflect random spatial patterns. Statistical significance was evaluated at $p < 0.05$, with larger absolute Z-scores corresponding to stronger spatial clustering.

The Getis-Ord Gi* method was selected because it effectively captures localized spatial dependence, accounting for both the magnitude and spatial context of drought indicators. Compared with global statistics such as Moran's I, Gi* detects fine-scale clustering of extremes (Akhter and Afroz, 2024; Nejadrekabi et al., 2021), making it particularly suitable for identifying regions with persistently high drought stress. This approach has been widely used in environmental and climate risk analyses for detecting areas of recurrent hazard concentration (Azeez et al., 2025; Nejadrekabi et al., 2021; Rousta et al., 2017).

3.3.4. Trend analysis

Temporal trends in SPEI and derived drought characteristics were analyzed using the Mann–Kendall test (Kendall, 1975; Mann, 1945; Haidu, 1997; Haidu & Magyari-Sáska, 2009) and Sen's slope estimator (Sen, 1968). The Mann–Kendall test is a non-parametric approach that determines the direction and significance of trends without requiring data normality. It is robust to missing values and outliers, making it suitable for climatological time series. Sen's slope estimator provides the rate of change by computing the median of all pairwise slopes between observations, thereby reducing the influence of extreme values and non-uniform sampling. All results were visualized in MATLAB's geospatial mapping toolbox using interpolation and k-means clustering to enhance spatial representation.

4. RESULTS

4.1. Model bias correction and validation

Fig. 2 illustrates the distributional comparison between observed, modelled, and bias-adjusted SPEI-03 values. The upper panel shows histograms, while the lower panel presents the corresponding KDE. Before bias correction, both historical and future modelled SPEI values exhibited systematic deviations from the observed distribution, with noticeable shifts around the mean and differences in tail behaviour. After applying EQM, the bias-adjusted SPEI distributions closely matched the observed pattern across the entire range of values. The KDE curves demonstrate a strong overlap between the observed (black line) and the historical bias-adjusted (purple) and future (blue) series.

This indicates a substantial correction of mean and variance biases. This alignment suggests that the EQM approach effectively removed systematic errors associated with the CanESM5 model, ensuring consistent representation of both dry (negative SPEI) and wet (positive SPEI) extremes. The strong correspondence between observed and adjusted datasets indicates that the CanESM5 outputs, after correction, are reliable for subsequent drought characterization and projection analysis.

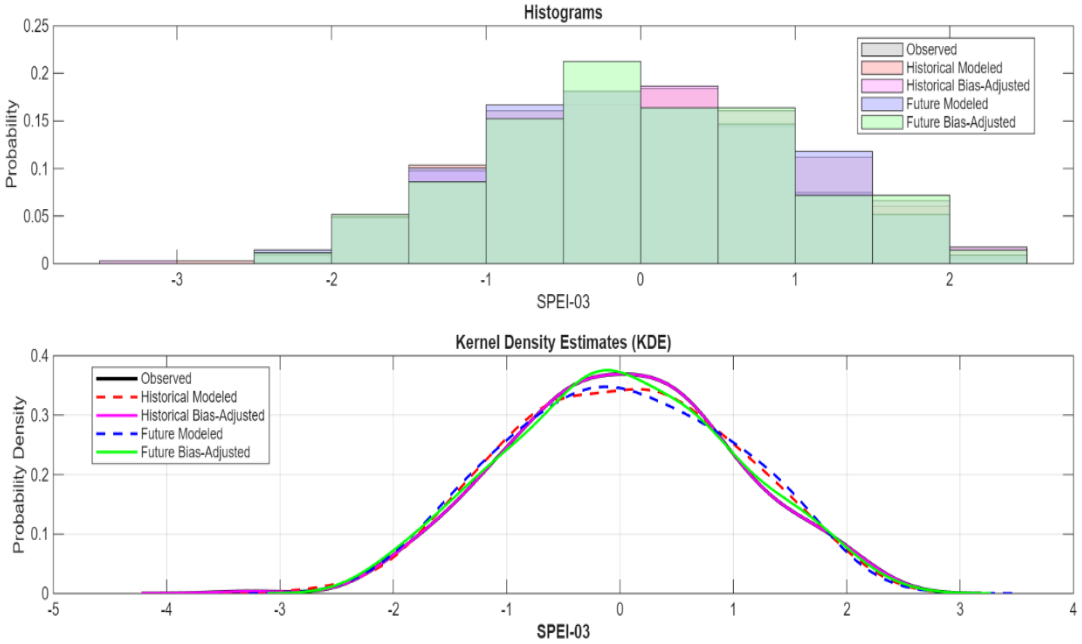

Fig. 2. Comparisons of observed, modeled, and bias-adjusted SPEI-03 distributions using histograms (top) and kernel density estimates (bottom).

4.2. Observed drought characteristics (1985-2014)

Fig. 3 illustrates the spatial distribution of historical drought duration, severity, intensity, and frequency across Uganda from 1985 to 2014, derived from SPEI-03. Observed drought duration (**Fig. 3a**) generally ranged between 2–4 months per event, with the longest durations (3–4 months) concentrated in the Southern Uganda and parts of Lake Victoria basin. The north, eastern and central regions exhibit relatively shorter events lasting 2–4 months. The spatial pattern of drought severity (**Fig. 3b**) indicates that the northwestern and central parts of Uganda experienced the most severe droughts, with mean severity values exceeding 1.5. In contrast, eastern and some parts of western Uganda show lower severity, suggesting that droughts there tend to be milder and shorter-lived.

Drought intensity (**Fig. 3c**), representing the average magnitude of water deficit per month, is highest across northwestern and some localized western parts of the country, with mean values approaching 0.7. Moderate intensity (0.4–0.6) occurs in the central, western, and parts of the Lake Victoria basin, whereas the northeastern, western highlands, and localized areas around Lake Victoria record the lowest intensities (≈0.3). This spatial pattern indicates that drought events exert stronger stress in the semi-arid north and southwestern subregions, consistent with their lower rainfall and higher evapotranspiration regimes.

Drought frequency (**Fig. 3d**) ranges between 10% and 25%, with the highest recurrence (>20%) observed across the northeastern, southern, southwestern, and Lake Victoria basin regions. The central parts of Uganda exhibit moderate frequencies (10–15%). This spatial pattern corresponds with historical records of recurrent droughts in the semi-arid north and the cattle corridor, highlighting these areas as long-standing zones of climatic stress.

Overall, the observed drought characteristics highlight a north–south gradient, with droughts becoming more frequent, severe, and intense toward the semi-arid north while the central remain relatively resilient. To further identify areas with spatial clustering of drought extremes, a hotspot analysis was conducted using the Getis-Ord Gi statistic based on drought frequency.

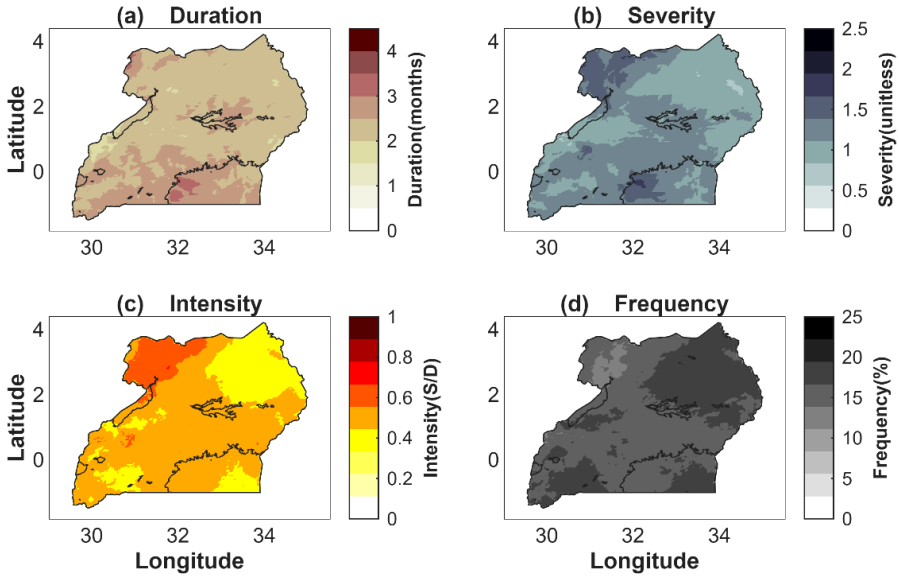

Fig. 3. Spatial distribution of observed drought characteristics across Uganda for 1985–2014 derived from SPEI-03: (a) drought duration (months), (b) drought severity (unitless), (c) drought intensity (average severity per drought month, S/D), and (d) drought frequency (%).

4.3. Observed drought hotspots

The observed drought hotspot analysis (**Fig. 4**) reveals distinct spatial clustering of historically drought-prone areas across Uganda. Significant hotspots are concentrated in the northeastern and eastern regions, covering parts of Teso, Lango, Acholi and much of Karamoja subregions. Additional clusters appear around the southwestern areas, particularly the Ankole subregion. All these areas fall within the famous Uganda's cattle corridor which has been severally reported as a drought hotspot. Another significant hotspot patch was revealed in the Lake Victoria basin. These areas represent zones with higher drought intensity and frequency, indicating persistent exposure to recurrent dry conditions. In contrast, most of central and northwestern Uganda show statistically insignificant patterns, suggesting relatively lower drought clustering during the observation period.

4.4. Observed SPEI-03 drought trends

The spatial pattern of the observed SPEI-03 (**Fig. 5**) shows that most parts of Uganda experienced increasing drought trends between 1985 and 2014. Results from the Mann–Kendall test indicate that the northern and western regions had statistically significant positive trends (stippling in **Fig 5**). This indicates that droughts have become more frequent and severe in these areas. The strongest drying is observed in northern Uganda, particularly in the Lango and Acholi subregions, where Sen's slope values exceed 8×10^{-5} units month^{-1}. In contrast, some parts of the southwestern highlands and the far northeast show decreasing drought tendencies, although these changes are not statistically significant and do not suggest a reversal of the overall trend. Overall, the findings suggest that Uganda has been getting progressively drier over the past four decades. The northern and western regions stand out as the most drought-prone zones. These are key agricultural and pastoral areas, implying growing vulnerability of rain-fed farming and livestock production to declining water availability.

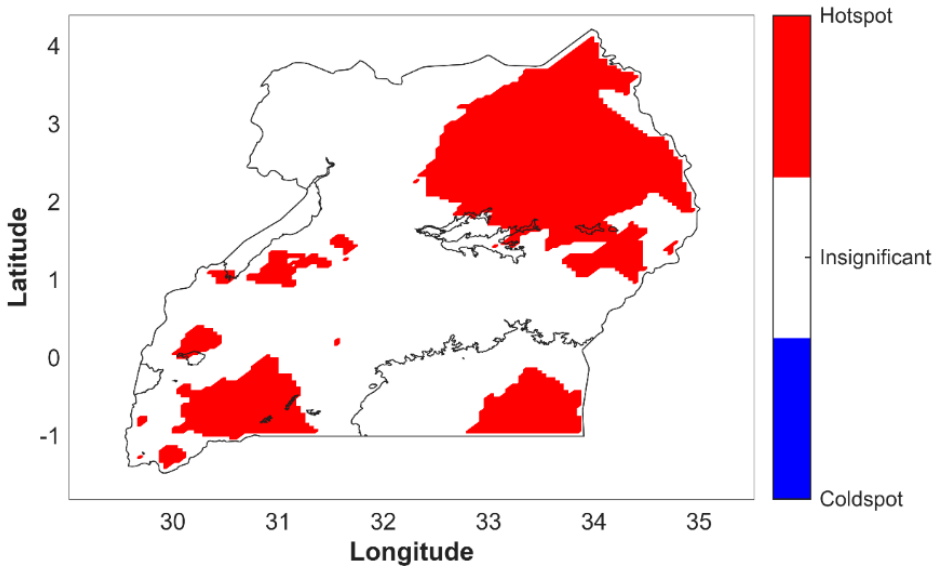

Fig. 4. Spatial distribution of drought hotspots across Uganda based on the Getis-Ord Gi* statistic derived from TerraClimate-based SPEI-03 data. Red areas indicate statistically significant drought hotspots ($p < 0.05$), blue areas represent cold spots, and white areas are insignificant regions.

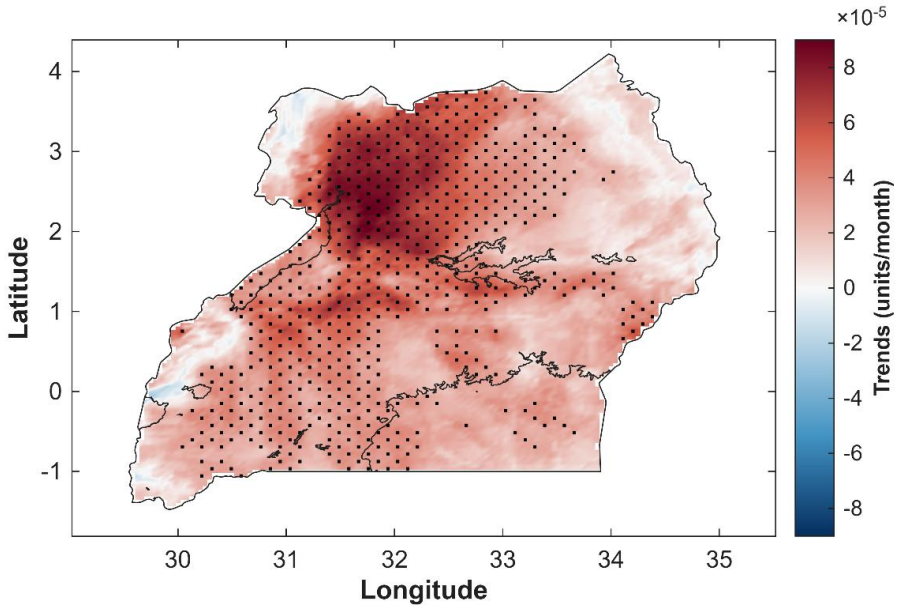

Fig. 5. Historical trends in SPEI-03 droughts (1985–2014) across Uganda derived from TerraClimate data. Stippling indicates areas where trends are statistically significant at $p < 0.05$ based on the Mann–Kendall test.

4.5. Projected drought characteristics

Projected drought characteristics exhibit substantial spatial and temporal variability across Uganda under the three emission scenarios (SSP1-2.6, SSP2-4.5, and SSP5-8.5) and two future periods (2041–2070 and 2071–2100). Generally, droughts are projected to become more frequent, longer, and more severe under higher-emission scenarios, especially toward the late century.

4.5.1. Duration

Projected drought duration shows distinct spatial and temporal variability across Uganda (**Fig. 6**). Under SSP1-2.6, droughts remain relatively short, averaging 1.5–2.5 months, with minimal spatial change throughout the century. In contrast, SSP2-4.5 projects longer droughts, particularly in northern Uganda, where the mean duration reaches 3–4 months during both mid- and late-century. Under SSP5-8.5, prolonged drought episodes expand toward central and western Uganda by the late century, with durations exceeding 3 months in several grid cells. Overall, longer drought events are projected under higher-emission scenarios, emphasizing increased persistence of dry spells with rising radiative forcing.

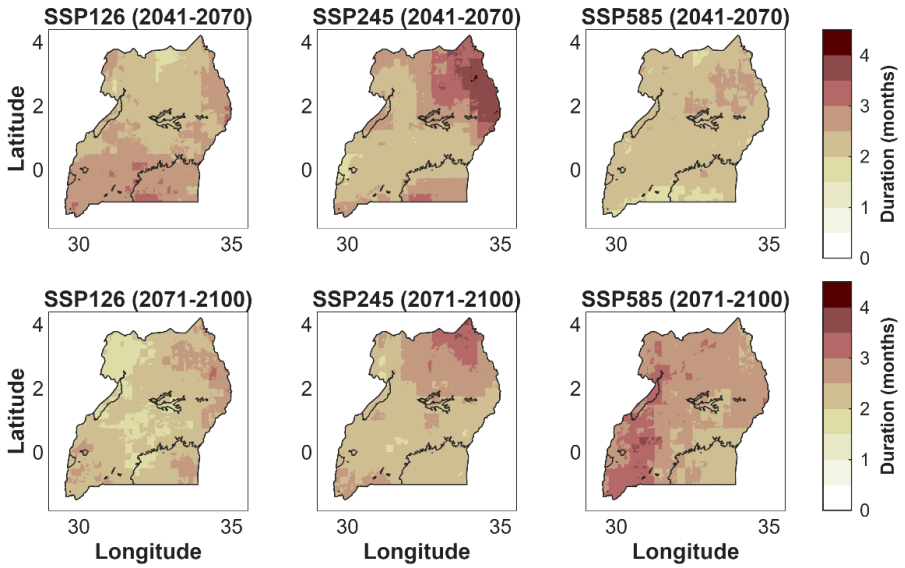

Fig. 6. Projected spatial distribution of mean drought duration (months) for SPEI-03 drought events in Uganda under three SSPs and two future periods. Top: mid-century (2041–2070); bottom: late-century (2071–2100).

4.5.2. Drought frequency

Projected drought frequency displays almost similar patterns in specific regions of the country (**Fig. 7**). Generally, drought occurrence remains moderate (10–15%) in the central and northwestern parts of the country throughout century. Higher recurrence is confined to the northeastern, southern and southwestern parts (up to 25%).

4.5.3. Drought severity

Projected drought severity exhibits clear spatial heterogeneity across Uganda, with the northern regions emerging as the most drought-prone areas (**Fig. 8**). During the mid-century period (2041–2070), drought severity across Uganda remains moderate under SSP1-2.6, with most areas exhibiting values below 1.5, except for localized areas of higher severity in the northwestern region. Under SSP2-4.5, severity increases markedly in the north, exceeding 1.5, suggesting longer and more intense dry episodes. Conversely, severity reduces under SSP5-8.5 for mid-century, showing values generally below 1.5 across the country. By the late century (2071–2100), drought severity slightly weakens nationwide under SSP1-2.6 and SSP2-4.5, indicating possible recovery under low-emission stabilization. However, there is intensification of severity under SSP5-8.5 across most parts of the country. The northwestern region experiences a clear intensification, with severity values surpassing 2.0, implying the occurrence of more extreme and prolonged droughts. Meanwhile, the southern and parts of the central regions maintain lower severity levels. These findings reveal a northward shift and amplification of drought severity under intermediate to high emission scenarios.

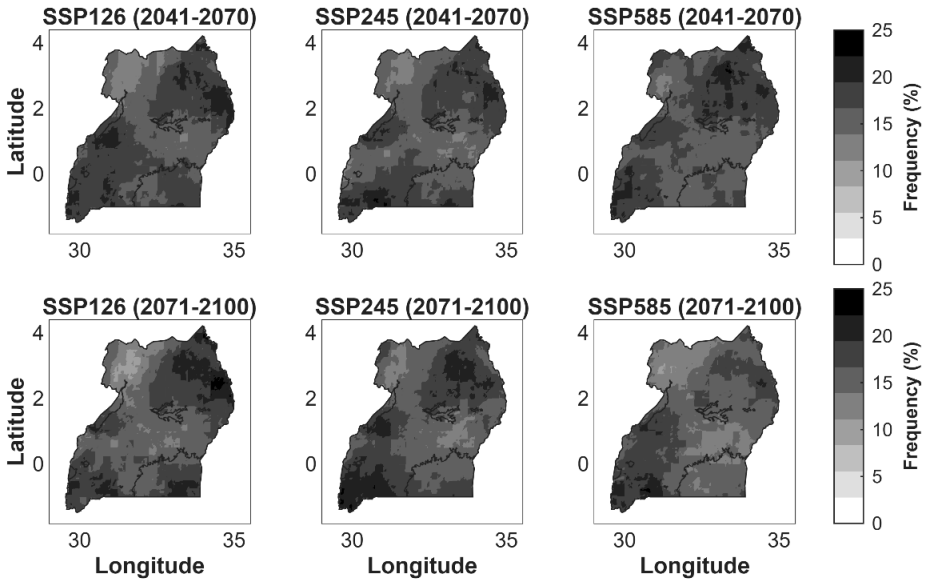

Fig. 7. Projected spatial distribution of drought frequency (%) across Uganda under three SSP scenarios for mid-century (2041-2070, top) and late century (2071-2100, bottom). Darker shades indicate higher drought recurrence based on SPEI ≤ –1

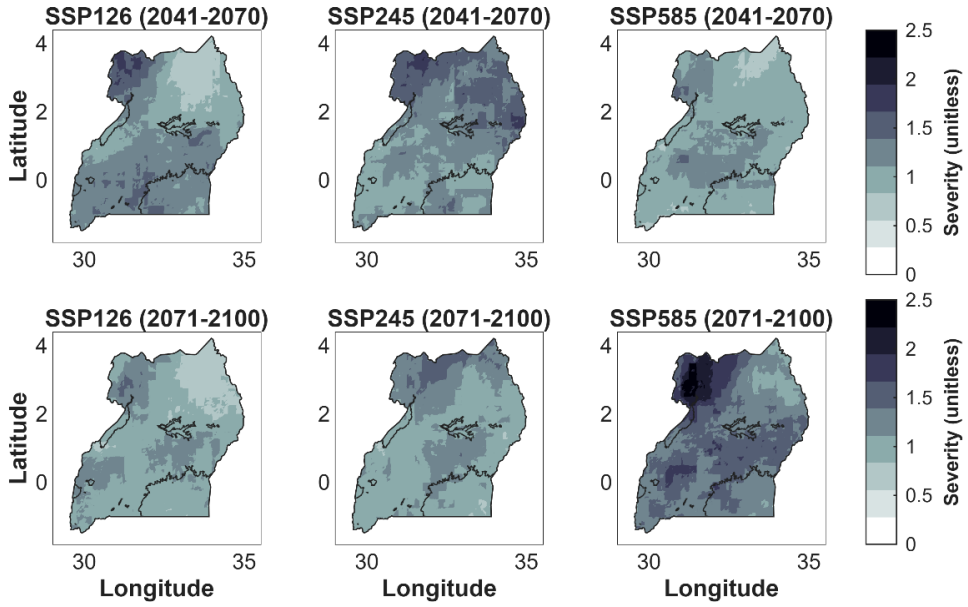

Fig. 8. Projected spatial distribution of drought severity across Uganda under SSP1-2.6, SSP2-4.5, and SSP5-8.5 for mid-century (2041–2070, top) and late-century (2071–2100, bottom). Darker shades indicate higher drought severity.

4.5.4. Drought intensity

During the mid-century (2041–2070), drought intensity is highest in the northwestern parts, with S/D values commonly between 0.5 and 0.8 under all the SSPs (**Fig. 9**). The central, western, and

southern Uganda remains moderate (≈0.3–0.5). By the late century (2071–2100), intensity increases and broadens under SSP5-8.5, exhibiting the strongest amplification, with extensive areas in the north, central, and eastern regions reaching S/D ≈0.7–1.0. These patterns indicate that, under higher emissions, drought months are projected to become substantially more severe on average, posing greater stress to agriculture and water resources.

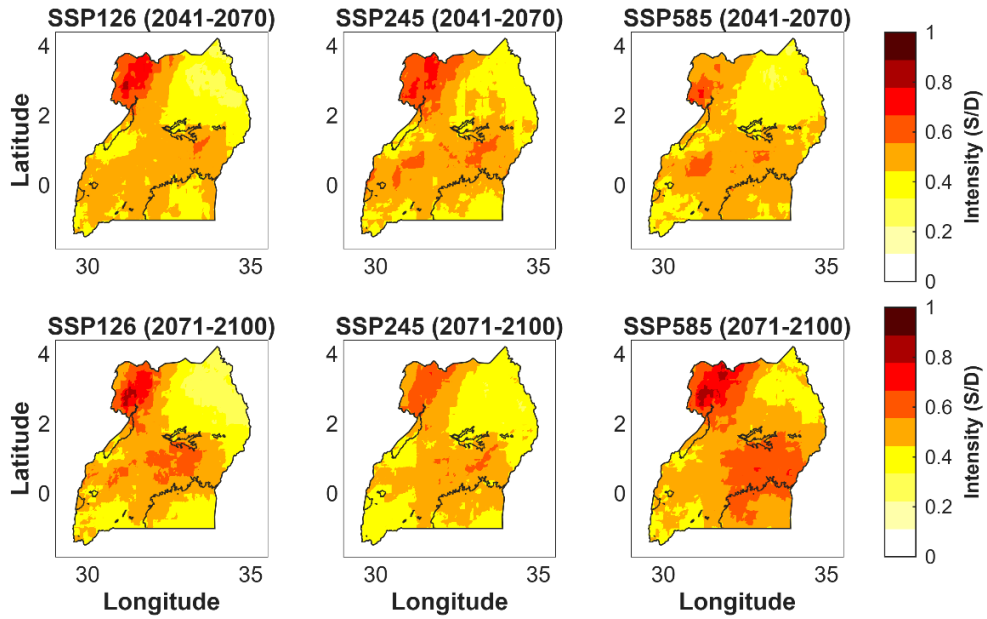

Fig. 9. Projected spatial distribution of drought intensity (average severity per drought month, S/D) for mid-century (2041–2070, top row) and late-century (2071–2100, bottom row) under SSP1-2.6, SSP2-4.5 and SSP5-8.5. Higher S/D values (darker red) indicate stronger average monthly drought deficits.

4.6. Projected hotspots

The Getis-Ord Gi* spatial statistic identified statistically significant and persistent drought hotspots primarily concentrated in northeastern, western and southwestern Uganda for the entire century (**Fig. 10**). This is particularly across the Karamoja, Kigezi and Ankole sub regions. These regions, which form the core of Uganda's cattle corridor, exhibited recurrent spatial clustering of high drought intensity and frequency ($p < 0.05$). Additional hotspot clusters were observed around the Lake Victoria basin, particularly under low emission scenarios for both mid and late centuries, reflecting localized drought susceptibility in this humid zone. They become less extensive under high emission scenarios.

The spatial persistence of these hotspots from the mid-century (2041–2070) to the late-century (2071–2100) periods suggests a sustained spatial anomaly in drought occurrence relative to surrounding areas. In certain areas, such as the northeastern and western zones, hotspots expand and intensify. In others, particularly parts of the Lake Victoria basin and eastern Uganda, they shrink or shift, suggesting evolving drought regimes.

The alignment of these statistically significant clusters with key agricultural and pastoral landscapes indicates that drought risks in these regions are likely to remain recurrent under future climatic conditions. This necessitates targeted adaptation strategies focused on water resource management, livestock systems, and agricultural resilience.

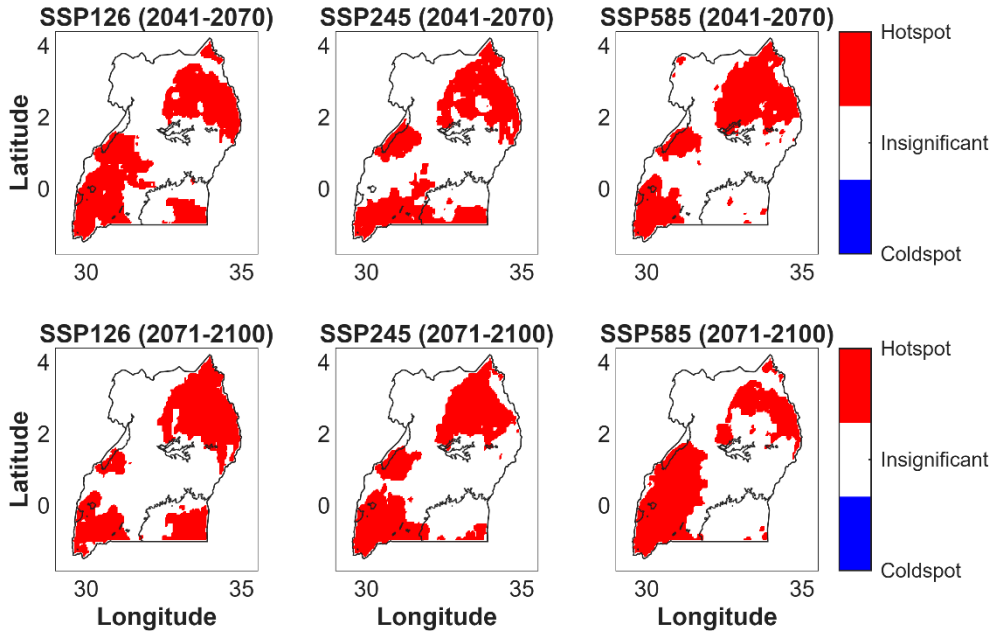

Fig. 10. Projected drought hotspot clusters (Getis-Ord Gi*, $p < 0.05$) for mid-century (2041–2070, top row) and late-century (2071–2100, bottom row) under SSP1-2.6, SSP2-4.5 and SSP5-8.5. Red indicates statistically significant drought hotspots; blue indicate cold spots and white indicates areas with insignificant hotspots.

4.7. Projected drought trends under different SSP scenarios

Projected SPEI-03 drought trends show marked spatial variability across Uganda, with the direction and magnitude of change differing between the mid-century (2041–2070) and late-century (2071–2100) periods across all emission scenarios (**Fig. 11**).

During the mid-century, drought occurrence significantly increases under SSP1-2.6, especially across central and northern Uganda, including areas around Lake Kyoga and the upper northern districts. Under SSP2-4.5, significant decreases in drought occurrence are projected across the central–western stretch of the country, while isolated increases persist over the Kyoga–Teso subregion. The high-emission SSP5-8.5 scenario, meanwhile, projects significantly decreasing drought trends over the Karamoja region in northeastern Uganda, suggesting localized improvement in short-term moisture conditions.

By the late century, the spatial configuration of droughts changes considerably. Under SSP1-2.6, most of the country experiences decreasing drought trends, especially across the western highlands, Lake Victoria basin, and northern zones. SSP2-4.5 exhibits a contrasting spatial pattern, with increasing drought trends concentrated in eastern Uganda, while decreasing trends dominate the West Nile. In contrast, the high-emission SSP5-8.5 scenario is dominated by significant increases in drought occurrence across southern, western, southwestern, and northern Uganda. These widespread positive trends indicate that droughts are projected to intensify and occur more frequently by the end of the century. Overall, the strongest increasing trends are projected under SSP5-8.5 during the late-century period, underscoring heightened drought risks under high-emission pathways.

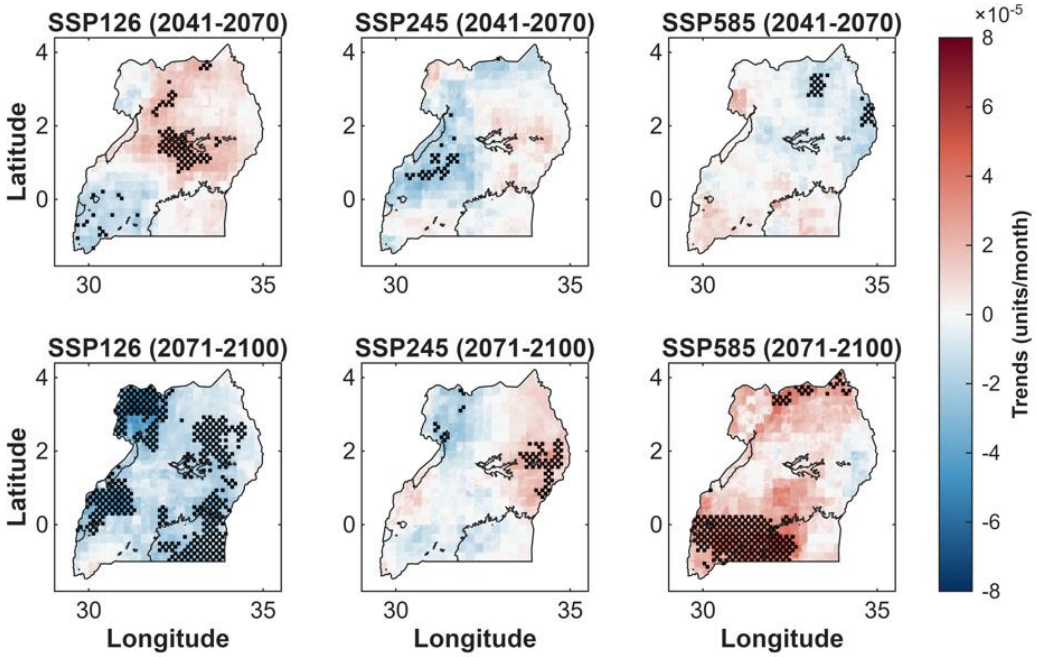

Fig. 11. Projected SPEI-03 trends across Uganda under SSP1-2.6, SSP2-4.5, and SSP5-8.5 for mid-century (2041–2070) and late-century (2071–2100) periods. Stippled areas denote statistically significant changes ($p < 0.05$).

5. DISCUSSION

5.1. Spatial and temporal dynamics of drought in Uganda

This study reveals that drought patterns in Uganda exhibit regional, scenario, and temporal variations. Under SSP1-2.6, drought occurrence increases during the mid-century in central and northern Uganda but decreases toward the late century. Under SSP2-4.5, droughts decrease in the central and western regions during the mid-century, then increase in eastern Uganda by the late century. Under SSP5-8.5, droughts decrease in Karamoja during the mid-century but become widespread and intense across the north, west, and south toward the late century. These shifts reflect the strong influence of rising temperatures and higher evapotranspiration (Ojara et al., 2024), which can offset rainfall gains and produce uneven drought outcomes.

The semi-arid north remains the most sensitive region. Droughts there often last two to four months and occur more frequently than in other parts of the country. This supports earlier evidence that Karamoja and the surrounding districts face persistent agricultural and hydrological droughts linked to short wet seasons and delayed rainfall onset (Byakatonda et al., 2021). Central and northwestern Uganda also shows signs of increasing drought risk, in line with past assessments by Kyatengerwa et al., (2020).

Hotspot analysis confirms that drought clusters remain strongest in the cattle corridor and extend from southwestern Uganda through the west and into the northeast. These are critical regions that support mixed farming and livestock. Mulinde et al., (2016) similarly identified the cattle corridor as a major climate risk zone due to its frequent dry spells and limited water storage capacity. Nalwanga et al., (2024) also reported that droughts in this region often persisted for several months, occasionally extending over multiple years under high-emission conditions. The persistence of these hotspots across scenarios and time periods suggests that drought risk is entrenched and unlikely to diminish. The Lake Victoria basin also exhibits localised hotspots in several scenarios, highlighting the sensitivity of this humid zone to short dry spells.

Across the country, drought patterns do not follow a single direction. Some regions experience temporary reductions in drought severity, particularly under SSP1-2.6 and mid-century SSP5-8.5, while others show apparent intensification. This mixed response aligns with the East African climate paradox, where rainfall may increase in parts of the region, but water stress still rises due to warming. Uganda's future drought landscape will therefore be shaped by localised hotspots rather than uniform drying. These areas, particularly the cattle corridor, Lake Victoria basin, and Karamoja, already experience livelihood stress (Nalwanga et al., 2025). Therefore, they should remain priority zones for targeted adaptation, improved water management, and climate-resilient livelihood strategies.

5.2. Contributions

High-resolution drought modelling using NEX GDDP CMIP6 downscaled to about 4 km for detailed national analysis. Integration of multiple drought metrics and hotspot detection to identify not only where droughts intensify but also where they cluster persistently in the whole country.

Scenario-based insights that show how drought patterns may diverge under low and high emissions, providing valuable input for policy and planning. Clear linkage between mapped hotspots and key livelihood zones that need targeted adaptation.

5.3. Limitations and future work

The analysis used a single GCM (CanESM5) from NEX-GDDP-CMIP6, which does not capture inter-model variability and uncertainty. Although the spatial resolution was improved through downscaling, localised microclimatic variations, especially in complex terrains such as highlands, may not be fully resolved. Future work should utilise multi-model ensembles and incorporate soil moisture, runoff, and vegetation indices to deepen the understanding. Linking drought metrics to crop yield, livestock loss, and water supply impacts would strengthen the practical value of the results. Including socioeconomic exposure and vulnerability data would also improve national drought risk assessments.

6. CONCLUSIONS

This study provides a national-scale assessment of historical and future droughts in Uganda using bias-adjusted CanESM5 data and SPEI. The combination of TerraClimate observations and downscaled projections produced a consistent picture of drought behavior across the country. Historical analysis shows strong drying in the north and parts of central Uganda. Future patterns differ across scenarios and time periods. Under SSP1-2.6, drought conditions remain mild except for a mid-century increase in central and northern Uganda. Under SSP2-4.5, droughts decrease in the central west during the mid-century but increase in eastern Uganda toward the late century. Under SSP5-8.5, droughts weaken in Karamoja during the mid-century but intensify across the north, west, and south by the end of the century.

Hotspot analysis reveals persistent clusters along the cattle corridor, extending from the Ankole and Kigezi regions to the west, through to Karamoja. These clusters indicate long-term drought stress in areas that depend on rainfed farming and pastoralism. The duration and frequency of droughts in these zones point to limited recovery capacity under future warming. Uganda's drought future is therefore uneven, with risks concentrated in specific agroecological regions. These findings support the need for locally tailored adaptation strategies and improved water management. They also emphasize the importance of integrating fine-scale climate information with agricultural systems, livestock, and livelihood resilience planning.

ACKNOWLEDGEMENTS

The corresponding author wishes to thank for the support from the European Commission through the Erasmus+ KA171 program which enabled the contribution to the development of education and research in the partner country Uganda. Dimitrie Cantemir University IR-BE-200465 project provided funding for the open access publication of this paper.

REFERENCES

Abatzoglou JT, Dobrowski SZ, Parks SA, et al. (2018) TerraClimate, a high-resolution global dataset of monthly climate and climatic water balance from 1958–2015. *Scientific Data* 5(1): 170191.

Ahmad MI, Sinclair CD and Werritty A (1988) Log-logistic flood frequency analysis. *Journal of Hydrology* 98(3–4): 205–224.

Akhter J and Afroz R (2024) Influence of climate variability and land cover dynamics on the spatio-temporal NDVI patterns in western hydrological regions of Bangladesh. *Heliyon* 10(12): e32625.

Akinsanola AA, Ongoma V and Kooperman GJ (2021) Evaluation of CMIP6 models in simulating the statistics of extreme precipitation over Eastern Africa. *Atmospheric Research* 254: 105509.

Allen RG, Raes D, Smith M, et al. (1998) *Crop Evapotranspiration : Guidelines for Computing Crop Water Requirements*. F.A.O.

Ayugi B, Shilenje ZW, Babaousmail H, et al. (2022) Projected changes in meteorological drought over East Africa inferred from bias-adjusted CMIP6 models. *Natural Hazards* 113(2). Springer Science and Business Media B.V.: 1151–1176.

Azeez M, Al Sharaa H and Ziboon AR (2025) Mapping agricultural lands at risk of meteorological drought in iraq using geostatistics. *Engineering and Technology Journal* 0(0): 1–14.

Baogang Y, Linxiao W, Hongyu T, et al. (2024) Future changes in extremes across China based on NEX-GDDP-CMIP6 models. *Climate Dynamics*. Springer Science and Business Media Deutschland GmbH. Epub ahead of print 1 October 2024. DOI: 10.1007/s00382-024-07408-7.

Byakatonda J, Openy G, Sempewo JI, et al. (2021) Over a century evidence of historical and recent dryness/wetness in sub-humid areas: A Uganda, East African case. *Meteorological Applications* 28(5).

Byamukama O, Ridwan WA and Biney MA (2025) Sustainability assessment of Uganda's Mabira, Budongo, and Kibale forest reserves. *Discover Environment* 3(1): 131.

Calverley CM and Walther SC (2022) Drought, water management, and social equity: Analyzing Cape Town, South Africa's water crisis. *Frontiers in Water* 4.

Ceola S, Mård J and Di Baldassarre G (2023) Drought and Human Mobility in Africa. *Earth's Future* 11(12). de Mendonça LM, Blanco CJC and da Silva Cruz J (2024) Performance and projections of the NEX-GDDP-CMIP6 in simulating precipitation in the Brazilian Amazon and Cerrado biomes. *International Journal of Climatology* 44(11): 3726–3741.

Dufatanye Umwali E, Chen X, Odhiambo Ayugi B, et al. (2024) Estimating the Effects of Climate Fluctuations on Precipitation and Temperature in East Africa. *Atmosphere* 15(12): 1455.

Elkouk A, El Morjani ZEA, Pokhrel Y, et al. (2021) Multi-model ensemble projections of soil moisture drought over North Africa and the Sahel region under 1.5, 2, and 3 °C global warming. *Climatic Change* 167(3–4): 52.

Ernawati NM, Torpan A, Voda M (2018) Geomedia role for Mountain Routes Development. Mesehe and Pisoiu Waterfall comparative study. *Geographia Technica* 13(1), 41-51.

Getis A and Ord JK (1992) The Analysis of Spatial Association by Use of Distance Statistics. *Geographical Analysis* 24(3): 189–206.

Haidu, I., (1997) Analiza seriilor de timp. Aplicatii în hidrologie. (*Time series analysis. Applications in hydrology* In romanian). Editura *H*G*A*, Bucuresti. ISBN: 973-98077-39. https://www.researchgate.net/publication/297032182_Analiza_seriilor_de_timp_Aplicatii_in_hidrologie

Haidu I. & Magyari-Sáska Z. (2009) *Animated sequential trend signal detection in finite samples*, Proceedings of the ITI 2009, 31st *International Conference on Information Technology Interfaces*, Cavtat, Croatia, Publisher: IEEE, pp. 249-254, DOI: 10.1109/ITI.2009.5196088.

Han X, Li Y, Yu W, et al. (2022) Attribution of the Extreme Drought in the Horn of Africa during Short-Rains of 2016 and Long-Rains of 2017. *Water* 14(3): 409.

IPCC (2022) *Technical Summary Frequently Asked Questions Part of the Working Group II Contribution to the Sixth Assessment Report of the Intergovernmental Panel on Climate Change*. Available at: www.environmentalgraphiti.org.

Jury MR (2018) Uganda rainfall variability and prediction. *Theoretical and Applied Climatology* 132(3–4): 905–919.

Kendall (1975) *Rank Correlation Methods*. 4th ed. London: Charles Griffin.

Kobusinge J, Twesigye CK, Kagezi GH, et al. (2024) Soil Moisture Content Suitability for Coffee Growing under Climate Change East African Scholars Journal of Agriculture and Life Sciences Soil Moisture Content Suitability for Coffee Growing under Climate Change Scenarios in Uganda. *East African Scholars Journal of Agriculture and Life Sciences* 7(11).

Kolling Neto A, Ribeiro RB, Fraga M de S, et al. (2024) Estimating water balance in a Brazilian semiarid watershed using different spatial data. *Journal of South American Earth Sciences* 140: 104930.

Krishna Prabhakar SVR (2022) Implications of Regional Droughts and Transboundary Drought Risks on Drought Monitoring and Early Warning: A Review. *Climate* 10(9): 124.

Kyatengerwa C, Kim D and Choi M (2020) A national-scale drought assessment in Uganda based on evapotranspiration deficits from the Bouchet hypothesis. *Journal of Hydrology* 580. Elsevier B.V.

Li X, Wu H, Nanding N, et al. (2023) Statistical Bias Correction of Precipitation Forecasts Based on Quantile Mapping on the Sub-Seasonal to Seasonal Scale. *Remote Sensing* 15(7). MDPI.

Li L, Du Q, Ren F, Huang L, Voda M, Ning P (2023) Geolocated social media data for measuring park visitation in Shenzhen, China, Urban Forestry & Urban Greening, Volume 88,128069, https://doi.org/10.1016/j.ufug.2023.128069

Lombe P, Carvalho E and Rosa-Santos P (2024) Drought Dynamics in Sub-Saharan Africa: Impacts and Adaptation Strategies. *Sustainability* 16(22): 9902.

Mann HB (1945) Nonparametric Tests Against Trend. *Econometrica* 13(3): 245.

Mathivha FI, Mabala L, Matimolane S, et al. (2024) El Niño-Induced Drought Impacts on Reservoir Water Resources in South Africa. *Atmosphere* 15(3): 249.

Mckee TB, Doesken NJ and Kleist J (1993) *The Relationship of Drought Frequency and Duration to Time Scales*. *Eighth Conference on Applied Climatology*.

Mulinde C, Mwanjalolo M and Egeru A (2016) *Meteorological Drought Occurrence and Severity in Uganda*. Available at: https://www.researchgate.net/publication/316701990.

Najjuma M, Nimusiima A, Sabiiti G, et al. (2021) Characterization of Historical and Future Drought in Central Uganda Using CHIRPS Rainfall and RACMO22T Model Data. *International Journal of Agriculture and Forestry* 2021(1): 9–15.

Nakalembe C (2018) Characterizing agricultural drought in the Karamoja subregion of Uganda with meteorological and satellite-based indices. *Natural Hazards* 91(3). Springer Netherlands: 837–862.

Nalwanga FS, Nanteza J, Obua J, et al. (2024) Insights into meteorological drought: navigating Uganda's cattle corridor through past trends and future projections. *Natural Hazards* 120(9). Springer Science and Business Media B.V.: 8695–8721.

Nalwanga FS, Kisira Y and Mukwaya PI (2025) Resilience to drought in Uganda's cattle corridor: gendered assets, expenditure, and decision-making. *BMC Environmental Science* 2(1). Springer Science and Business Media LLC.

Nejadrekabi M, Eslamian S and Zareian MJ (2021) Using spatial statistics to identify drought-prone regions (A case study of Khuzestan Province, Iran). *Advances in Environmental Technology* 7(4). Iranian Research Organization for Science and Technology: 231–262.

Ngoma H, Wen W, Ojara M, et al. (2021) Assessing current and future spatiotemporal precipitation variability and trends over Uganda, East Africa, based on CHIRPS and regional climate model datasets. *Meteorology and Atmospheric Physics* 133(3). Springer: 823–843.

Niranjan Kumar K, Thota MS, Ashrit R, et al. (2022) Quantile mapping bias correction methods to IMDAA reanalysis for calibrating NCMRWF unified model operational forecasts. *Hydrological Sciences Journal* 67(6): 870–885.

Nsubuga FW and Rautenbach H (2018) Climate change and variability: a review of what is known and ought to be known for Uganda. *International Journal of Climate Change Strategies and Management* 10(5): 752–771.

Nuwagira U and Yasin I (2022) Review of the Past, Current, and the Future Trend of the Climate Change and its Impact in Uganda. *East African Journal of Environment and Natural Resources* 5(1): 115–126.

Ojara MA, Babaousmail H, Aribo L, et al. (2024) Patterns of rainfall and temperature and their relationships with potential evapotranspiration rates over the period 1981–2022 in parts of central, western, southern, and southwestern Uganda. *Environmental Monitoring and Assessment* 196(10): 898.

Onyeaka H, Nwauzoma UM, Akinsemolu AA, et al. (2024) The ripple effects of climate change on agricultural sustainability and food security in Africa. *Food and Energy Security* 13(5).

Onyutha C and Kerudong PA (2022) Changes in Meteorological Dry Conditions across Water Management Zones in Uganda. *KSCE Journal of Civil Engineering* 26(12). Korean Society of Civil Engineers: 5384–5403.

Orimoloye IR, Belle JA, Orimoloye YM, et al. (2022) Drought: A Common Environmental Disaster. *Atmosphere* 13(1): 111.

Orke YA and Li M-H (2022) Impact of Climate Change on Hydrometeorology and Droughts in the Bilate Watershed, Ethiopia. *Water* 14(5): 729.

Rao KK, Al Mandous A, Al Ebri M, et al. (2024) Future changes in the precipitation regime over the Arabian Peninsula with special emphasis on UAE: insights from NEX-GDDP CMIP6 model simulations. *Scientific Reports* 14(1): 151.

Rousta I, Doostkamian Mehdi, Haghighi Esmaeil, et al. (2017) Analysis of Spatial Autocorrelation Patterns of Heavy and Super-Heavy Rainfall in Iran. *ADVANCES IN ATMOSPHERIC SCIENCES* 34(9): 1069–1081.

Samuel S, Mengistu Tsidu G, Dosio A, et al. (2025) Assessment of Historical and Future Mean and Extreme Precipitation Over Sub-Saharan Africa Using NEX-GDDP-CMIP6: Part I—Evaluation of Historical Simulation. *International Journal of Climatology* 45(2).

Satoh Y, Yoshimura K, Pokhrel Y, et al. (2022) The timing of unprecedented hydrological drought under climate change. *Nature Communications* 13(1): 3287.

Sen PK (1968) Estimates of the Regression Coefficient Based on Kendall's Tau. *Journal of the American Statistical Association* 63(324): 1379–1389.

Ssembajwe R, Mulinde C, Ddumba SD, et al. (2024) Dynamics and associations of selected agrometeorological variables in Robusta growing regions of Uganda. *Agricultural Water Management* 307: 109257.

Ssembajwe R, Twah A, Kagezi GH, et al. (2025) Assessment and Validation of FAPAR, a Satellite-Based Plant Health and Water Stress Indicator, over Uganda. *Remote Sensing* 17(20): 3501.

Ssembajwe R, Ngatia M, Kagezi GH, et al. (2025) Evaluation of gridded and reanalysis vapour pressure deficit datasets over East Africa. *Journal of Southern Hemisphere Earth Systems Science* Drumond A (ed.) 75(3).

Ssembajwe R, Nguefack J, Mezafack KL, et al. (2025) Spatiotemporal dynamics and drivers of agricultural droughts in the agroecological zones of Cameroon. *International Journal of Applied Earth Observation and Geoinformation* 140: 104581.

Ssembajwe Ronald, Twah A, Nakabugo R, et al. (2025) Wind and Humidity Nexus over Uganda in the Context of Past and Future Climate Volatility. *Climate* 13(5): 86.

Thrasher B, Wang W, Michaelis A, et al. (2022) NASA Global Daily Downscaled Projections, CMIP6. *Scientific Data* 9(1): 262.

UBOS (2024) *Uganda Annual Agricultural Survey 2021/22*. Kampala. Available at: https://www.ubos.org/wp-content/uploads/publications/UHIS_2021_22-Report-Final.pdf (accessed 14 November 2025).

UBOS (2025) Uganda Profile. Available at: https://www.ubos.org/uganda-profile/ (accessed 14 November 2025).

Uwimbabazi J, Jing Y, Iyakaremye V, et al. (2022) Observed Changes in Meteorological Drought Events during 1981–2020 over Rwanda, East Africa. *Sustainability* 14(3): 1519. 17.

Voda M, Kithiia S, Jackiewicz E, Du Q, Sarpe CA (2019) Geosystems 'pathways to the future of Sustainability, *Scientific reports*, 9(1), 1-11. https://www.nature.com/articles/s41598-019-50937-z

Voda AI, Sarpe CA, and Voda M (2018). Methods of maximum discharge computation in ungauged river basins. Review of procedures in Romania. *Geographia Technica*, 13(1), 130-137.

Vicente-Serrano SM, Beguería S and López-Moreno JI (2010) A multiscalar drought index sensitive to global warming: The standardized precipitation evapotranspiration index. *Journal of Climate* 23(7): 1696–1718.

Vinodhkumar B, Ullah S, Kumar TVL, et al. (2024) Amplification of temperature extremes in Arabian Peninsula under warmer worlds. *Scientific Reports* 14(1): 16604.

Wang Q, Zeng J, Qi J, et al. (2021) A multi-scale daily SPEI dataset for drought characterization at observation stations over mainland China from 1961 to 2018. *Earth System Science Data* 13(2). Copernicus Publications: 331–341.

Wu F, Jiao D, Yang X, et al. (2023) Evaluation of NEX-GDDP-CMIP6 in simulation performance and drought capture utility over China – based on DISO. *Hydrology Research* 24(5). IWA Publishing: 703–721.

Yevjevich (1967) *An Objective Approach to Definitions and Investigations of Continental Hydrologic Droughts*.